



Luminous Radio Emission from the Superluminous Supernova 2017ens at 3.3 yr after Explosion

Raffaella Margutti^{1,2}, J. S. Bright^{1,3}, D. J. Matthews¹, D. L. Coppejans⁴, K. D. Alexander⁵, E. Berger⁶, M. Bietenholz⁷, R. Chornock¹, L. DeMarchi⁸, M. R. Drout⁹, T. Eftekhari^{10,23}, W. V. Jacobson-Galán^{1,24}, T. Laskar^{11,12}, D. Milisavljevic^{13,14}, K. Murase^{15,16,17}, M. Nicholl¹⁸, C. M. B. Omand¹⁹, M. Stroh¹⁰, G. Terreran^{20,21}, and B. A. VanderLey²²

¹ Department of Astronomy, University of California, Berkeley, CA 94720-3411, USA; rmargutti@berkeley.edu

² Department of Physics, University of California, 366 Physics North MC 7300, Berkeley, CA 94720, USA

³ Astrophysics, Department of Physics, University of Oxford, Keble Road, Oxford OX1 3RH, UK

⁴ Department of Physics, University of Warwick, Coventry CV4 7AL, UK

⁵ Department of Astronomy/Steward Observatory, 933 North Cherry Avenue, Rm. N204, Tucson, AZ 85721-0065, USA

⁶ Center for Astrophysics, Harvard & Smithsonian, 60 Garden Street, Cambridge, MA 02138-1516, USA

⁷ SARAO/Hartebeesthoek Radio Observatory, PO Box 443, Krugersdorp 1740, South Africa

⁸ Astronomer-in-Residence at Department of Physics Boise State University, 1910 University Drive, Boise, ID 83725-1570, USA

⁹ David A. Dunlap Department of Astronomy and Astrophysics, University of Toronto 50 St. George Street, Toronto, Ontario, M5S 3H4, Canada

¹⁰ Center for Interdisciplinary Exploration and Research in Astrophysics (CIERA) and Department of Physics and Astronomy, Northwestern University, Evanston, IL 60208, USA

¹¹ Department of Physics & Astronomy, University of Utah, Salt Lake City, UT 84112, USA

¹² Department of Astrophysics/IMAPP, Radboud University, P.O. Box 9010, 6500 GL, Nijmegen, The Netherlands

¹³ Purdue University, Department of Physics and Astronomy, 525 Northwestern Avenue, West Lafayette, IN 47907, USA

¹⁴ Integrative Data Science Initiative, Purdue University, West Lafayette, IN 47907, USA

¹⁵ Department of Physics, Department of Astronomy & Astrophysics, & Center for Multimessenger Astrophysics, Institute for Gravitation & the Cosmos, The Pennsylvania State University, University Park, PA 16802, USA

¹⁶ School of Natural Sciences, Institute for Advanced Study, Princeton, NJ 08540, USA

¹⁷ Center for Gravitational Physics and Quantum Information, Yukawa Institute for Theoretical Physics, Kyoto, Kyoto 606-8502, Japan

¹⁸ Astrophysics Research Centre, School of Mathematics and Physics, Queens University Belfast, Belfast BT7 1NN, UK

¹⁹ The Oskar Klein Centre, Department of Astronomy, Stockholm University, AlbaNova, SE-106 91 Stockholm, Sweden

²⁰ Las Cumbres Observatory, 6740 Cortona Drive, Suite 102, Goleta, CA 93117-5575, USA

²¹ Department of Physics, University of California, Santa Barbara, CA 93106-9530, USA

²² National Science Foundation, 2415 Eisenhower Avenue, Alexandria, VA 22314, USA

Received 2023 June 23; revised 2023 August 10; accepted 2023 August 18; published 2023 September 11

Abstract

We present the results from a multiyear radio campaign of the superluminous supernova (SLSN) SN 2017ens, which yielded the earliest radio detection of an SLSN to date at the age of ~ 3.3 yr after explosion. SN 2017ens was not detected at radio frequencies in the first ~ 300 days but reached $L_\nu \approx 10^{28} \text{ erg s}^{-1} \text{ cm}^{-2} \text{ Hz}^{-1}$ at $\nu \sim 6$ GHz, ~ 1250 days post explosion. Interpreting the radio observations in the context of synchrotron radiation from the supernova shock interaction with the circumstellar medium (CSM), we infer an effective mass-loss rate $\dot{M} \approx 10^{-4} M_\odot \text{ yr}^{-1}$ at $r \sim 10^{17}$ cm from the explosion's site, for a wind speed of $v_w = 50\text{--}60 \text{ km s}^{-1}$ as measured from optical spectra. These findings are consistent with the spectroscopic metamorphosis of SN 2017ens from hydrogen poor to hydrogen rich ~ 190 days after explosion reported by Chen et al. SN 2017ens is thus an addition to the sample of hydrogen-poor massive progenitors that explode shortly after having lost their hydrogen envelope. The inferred circumstellar densities, implying a CSM mass up to $\sim 0.5 M_\odot$, and low velocity of the ejection suggest that binary interactions (in the form of common-envelope evolution and subsequent envelope ejection) play a role in shaping the evolution of the stellar progenitors of SLSNe in the $\lesssim 500$ yr preceding core collapse.

Unified Astronomy Thesaurus concepts: Core-collapse supernovae (304); Extragalactic radio sources (508)

1. Introduction

More than a decade after the identification of superluminous supernovae (SLSNe) as a new class of stellar explosions with peak bolometric luminosities $L_{\text{pk}} \sim 10\text{--}100$ times those of ordinary core-collapse supernovae (SNe; Chomiuk et al. 2011; Quimby et al. 2011), the nature of the energy source that

powers their exceptional optical display and of their progenitor stars are still debated (see, e.g., Moriya et al. 2018; Gal-Yam 2019 for recent reviews). Arguments based on the comparison between the observed rise time of SLSNe and the diffusion timescale of photons through the explosion's ejecta lead to the conclusion that the radioactive decay of large amounts (i.e., $>1 M_\odot$) of ^{56}Ni that was suggested, for example, in the case of SN 2007bi (Gal-Yam et al. 2009), is not a viable option for the entire class of SLSNe and that other sources of energy have to be invoked.

Alternatives include (i) the SN shock interaction with a dense medium (e.g., Chevalier & Irwin 2011) and/or (ii) a magnetar central engine (e.g., Kasen & Bildsten 2010; Woosley 2010). Both scenarios are expected to leave clear

²³ NASA Einstein Fellow.

²⁴ NSF Graduate Student Fellow.



imprints on the nonthermal spectrum of the source, as opposed to the UV/optical/near-infrared regime that is dominated by thermal processes and is not sensitive to the explosion’s fastest ejecta. Nonthermal processes, including the later-time breakout of the emission from a pulsar wind nebula (e.g., Omand & Jerkstrand 2023), are best constrained at radio frequencies. Yet, SLSNe have mostly eluded radio detection. So far, PTF10hgi was the only SLSN with any detected radio emission, with the first detection only at $\delta t_{\text{rest}} \sim 6.3$ yr after explosion (Eftekhari et al. 2019, 2021; Law et al. 2019; Mondal et al. 2020; Hatsukade et al. 2021a, 2021b). Here we present the results from a multiyear radio campaign on SN 2017ens, which led to the earliest radio detection of an SLSN to date at $\delta t_{\text{rest}} \sim 3.3$ yr after explosion (Coppejans et al. 2021a).²⁵

SN 2017ens (aka ATLAS17gqa) was discovered by the Asteroid Terrestrial-impact Last Alert System (ATLAS; Tonry et al. 2018) on 2017 June 5 and classified as a H-poor stellar explosion at $z = 0.1086$ by Chen et al. (2018) as part of the GREAT Survey. With a peak absolute magnitude $M_g = -21.1$ mag, SN 2017ens belongs to the class of SLSNe. Starting with blue featureless spectra until the time of maximum light, SN 2017ens later underwent a dramatic spectral evolution characterized by the appearance of prominent H lines of the Balmer series that displayed a broad emission component (FWHM of ~ 2000 km s⁻¹) and a low-velocity P-Cygni profile with $v \sim 50\text{--}60$ km s⁻¹ (Chen et al. 2018). Interestingly, Chen et al. (2018) also report the presence of coronal lines likely resulting from X-ray photoionization that are typically seen for some Type II In SNe (e.g., SN2010jl, Fransson et al. 2014). These spectral features and the significant flattening of the optical lightcurve at $\delta t_{\text{rest}} > 150$ days since explosion (see Figure 1 in Chen et al. 2018) are a clear indication of the SN shock interaction with a dense, H-rich circumstellar medium (CSM). The infrared (IR) brightening of SN 2017ens at a few hundred days post explosion reported by Sun et al. (2022) supports the presence of dust in the explosion’s surroundings. While the origin of the dust is debated (newly formed versus preexisting), IR excesses are routinely detected around SN shocks that interact with dense CSM (e.g., Tinyanont et al. 2019). SN shocks propagating into a dense CSM are also well-known particle accelerators and efficiently convert the explosion’s kinetic energy into heat (see, e.g., Chevalier & Fransson 2017 for a recent review), a process that leads to copious X-ray and radio emission that we study here.

We present radio observations of SN 2017ens spanning $\delta t = 55.0\text{--}1602$ days. This paper is organized as follows. In Section 2 we present the data analysis and reduction from our multiyear radio campaign of SN 2017ens. We model the radio data in Section 3 in the context of synchrotron emission from a blast wave propagating into the environment, and we discuss our findings in Section 4. Following Chen et al. (2018) we adopt $z = 0.1086$, which translates into a luminosity distance of $d_L = 490$ Mpc for a cosmological model with $H_0 = 72$ km s⁻¹ Mpc⁻¹, $\Omega_\Lambda = 0.73$, and $\Omega_m = 0.27$. Times, δt , are reported with respect to the explosion date, which is MJD $57,907.8 \pm 1.5$ (Chen et al. 2018), and in the observer frame, unless explicitly noted otherwise. We note that the small uncertainty on the explosion date has no impact on our conclusions.

²⁵ We note that further analysis and additional follow-up observations of the H-poor SLSN 2020tcw show that the radio emission that we reported in Coppejans et al. (2021b) is likely due to an unrelated source (D. Matthews et al. 2023, in preparation).

2. Data Analysis

We observed the field of SN 2017ens with the Karl G. Jansky Very Large Array (VLA) beginning on 2017 July 28 ($\delta t = 55.0$ days) as part of project 17A-480 (PI: D. L. Coppejans). We continued observing SN 2017ens with VLA programs 17B-225 (PI: R. Margutti), 20B-144 (PI: D. J. Matthews), and 21B-290 (PI: D. L. Coppejans). Overall, our multiyear radio monitoring spans the time period $\delta t = 55.0\text{--}1602$ days with the VLA in the A, B, and C configurations. We list the observing sessions in Table 1.

Data were calibrated using the Common Astronomy Software Applications (CASA, version 6.4.1.12; McMullin et al. 2007; CASA Team et al. 2022) VLA pipeline version 2022.2.06.64, which performs flagging, delay correction, bandpass and absolute flux density scaling, and phase-reference calibration. Imaging was performed either with the CASA TCLEAN task or WSClean (Offringa & Smirnov 2017) using Briggs weighting with a robust factor of 0.5.

We discovered significant radio emission from SN 2017ens on 2021 January 28 at $\delta t = 1334$ days (Coppejans et al. 2021a), with a flux density of $F_\nu = (38 \pm 5) \mu\text{Jy}$ at 6 GHz (a $\sim 7\sigma$ detection given the image noise of $5 \mu\text{Jy beam}^{-1}$). We show the discovery image in Figure 1. The position of the source is R.A. = $12^{\text{h}}04^{\text{m}}09^{\text{s}}384(1)$, decl. = $-01^{\circ}55'52''56(2)$, with the number in parentheses indicating the uncertainty in the last digit. We fit the flux density and position using the CASA task `IMFIT` by fitting to the image an elliptical Gaussian with dimensions fixed to those of the restoring (synthesized) beam, which has FWHM major and minor axes, and position angle of $0''.37$, $0''.29$, and $26^\circ 6$, respectively. The absolute positional accuracy of the VLA using standard phase-reference calibration techniques (as was the case for all our observations) and under typical conditions is $\sim 10\%$ of the synthesized beam, or $\sim 0''.03$ to $\sim 0''.04$ in this case. The optical position of SN 2017ens is R.A. = $12^{\text{h}}04^{\text{m}}09^{\text{s}}39(1)$, decl. = $-01^{\circ}55'52.5(2)''$, with the number in parentheses indicating the uncertainty in the last digit, as measured by the Gamma-Ray Burst Optical Near-infrared Detector (T.-W. Chen 2023, private communication), confirming the radio source is the counterpart to SN 2017ens. The optical source is also displaced compared to the host-galaxy center (Chen et al. 2018, their Figure 4). For observations taken after our initial detection we fit a point-source component fixed to the position found in our discovery image and report the forced-fit flux from this process. We present the results of our radio observations in Table 1. In the following we also use a 3σ upper limit of $F_\nu < 39.3 \mu\text{Jy}$ reported by Chandra et al. (2021) using a Giant Metrewave Radio Telescope observation on 03.85 March 2021 (MJD 59,281.85, $\delta t = 1374.050$ days) at 1.26 GHz. The complete set of radio observations is shown in Figure 2. We put the radio lightcurve of SN 2017ens in the context of those of other core-collapse stellar explosions in Figure 3.

3. Modeling of the Radio Emission

The emergence of detectable radio emission following the appearance of H lines in the spectrum suggests an origin of the radio emission connected with the interaction of the SN shock with a H-rich higher-density medium, in close similarity to other transitional events like SN 2014C (Milisavljevic et al. 2015; Margutti et al. 2017). We explore in Sections 3.1 and 3.2 the constraints on the CSM density and on relativistic jets that can be placed with our radio observations.

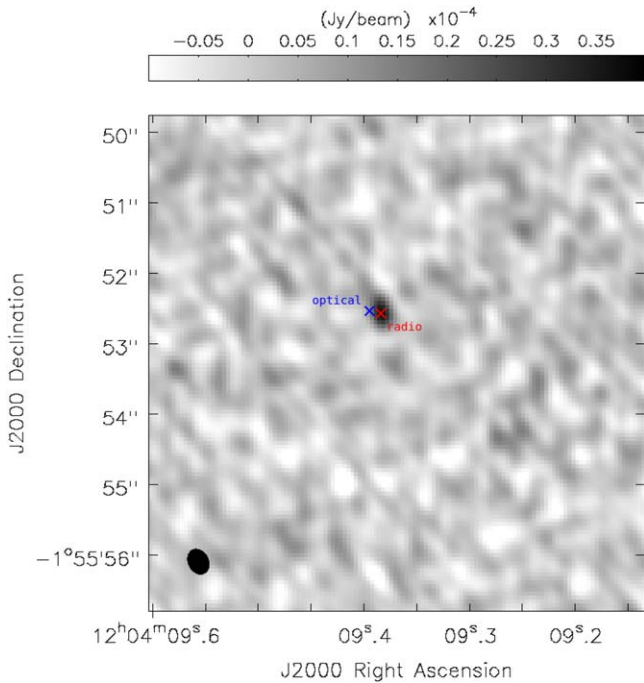


Figure 1. The field of SN 2017ens observed at 6 GHz with the VLA on 2021 January 28 showing the onset of radio emission from the source at $F_\nu = 38 \pm 5 \mu\text{Jy}$. The grayscale image shows flux density per beam and ranges between -10 and $40 \mu\text{Jy}$; the synthesized beam, with major and minor axes of $0''.37$ and $0''.29$ at a position angle of $26^\circ 6'$, is shown in black in the bottom left corner of the image. The red cross shows the radio position, R. A. = $12^{\text{h}}04^{\text{m}}09^{\text{s}}.384(1)$, decl. = $-01^\circ 55' 52.56(2)''$, which is consistent with the optical position of the transient, shown by the blue cross; see Section 2.

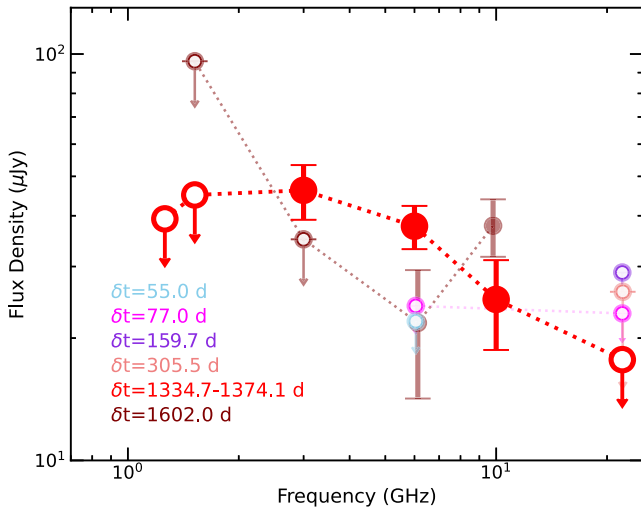


Figure 2. Temporal evolution of the radio spectral energy distribution (SED) of SN 2017ens in the time range $\delta t = 55\text{--}1602$ days. No radio emission is detected in the first year after explosion. Our first radio detection of SN 2017ens occurred at $\delta t \sim 1350$ days (red). Open symbols mark upper limits.

3.1. Constraints on the Environment Density

The deceleration of an SN shock in the CSM, and the resulting acceleration of particles at the SN shocks, is a well-known source of radio synchrotron emission in stellar explosions (e.g., Chevalier & Fransson 2017). In young SNe, the radio emission originates from the forward shock and creates a characteristic bell-shaped spectrum with the frequency

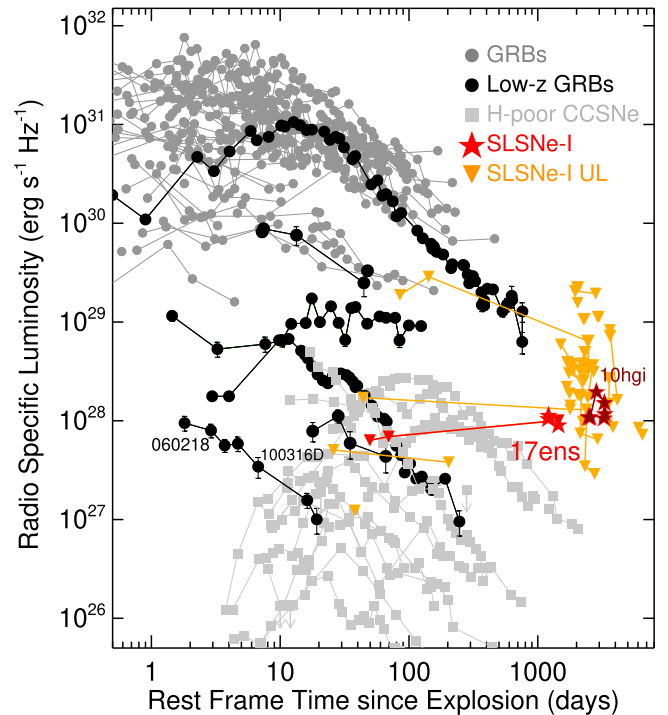


Figure 3. Radio specific luminosity L_ν from SN 2017ens in the context of other Type I super-luminous supernovae (SLSNe-I; triangles and stars for upper limits and measurements, respectively), normal H-poor core-collapse SNe (light gray squares), long GRBs at cosmological distances (dark gray dots) and in the local Universe (black dots) at $\nu \approx 6$ GHz rest frame. GRB and SN data collected from Soderberg et al. (2010), Chandra & Frail (2012), Margutti et al. (2014), and references therein. For SLSNe-I, we select observations carried out in the rest-frame frequency range 3–8 GHz. SLSNe-I references: Chandra et al. (2009, 2010), Chomiuk et al. (2011), Kasliwal et al. (2016), Nicholl et al. (2016, 2018), Bright et al. (2017), Bose et al. (2018), Coppejans et al. (2018), Hatsukade et al. (2018, 2021b), Schulze et al. (2018), Eftekhari et al. (2019, 2021), Law et al. (2019), Mondal et al. (2020), and Chandra et al. (2021).

of the spectral peak cascading down to lower values with time as the emission becomes optically thin, in the case of Type Ib/c SNe usually to synchrotron self-absorption (SSA). In the following we first assume that in the case of SN 2017ens, SSA dominates (i.e., that there is no significant free–free absorption, FFA), and we adopt the standard formulation of SSA emission in SNe by Chevalier (1998) and follow the formalism that we have developed in DeMarchi et al. (2022).²⁶

We start with considerations on the radio spectral energy distribution (SED) when we first detected the SN at $\delta t = 1334.7\text{--}1374.1$ days (Figure 2). If we define a power-law spectrum as one with $F_\nu \propto \nu^{-\beta}$, where β is the spectral index, then the observed values at $\delta t = 1334.7\text{--}1374.1$ days are not consistent with a single power law but rather imply $\beta \approx 0.5\text{--}1$ for $\nu \gtrsim 3.5$ GHz, with the upper limit at 22 GHz requiring $\beta \gtrsim 0.5$ and the upper limits at $\nu < 2$ GHz requiring a turnover somewhere below ~ 4 GHz. The observations at this epoch constrain the observed spectral peak flux density²⁷ to $40 \mu\text{Jy} \lesssim F_{\text{pk}} \lesssim 60 \mu\text{Jy}$ with the peak occurring in the range $1 \text{ GHz} \lesssim \nu_{\text{pk}} \lesssim 4 \text{ GHz}$. Assuming equipartition of energy

²⁶ Specifically, we used Equations (18), (19), (21), (26), and (27) from DeMarchi et al. (2022).

²⁷ Note that this value is the actual peak in the spectrum. The corresponding peak flux parameter that would go into the Chevalier (1998) equations, which is the intersection of the optically thick and optically thin asymptotes of the spectrum, is in the range 60–100 μJy .

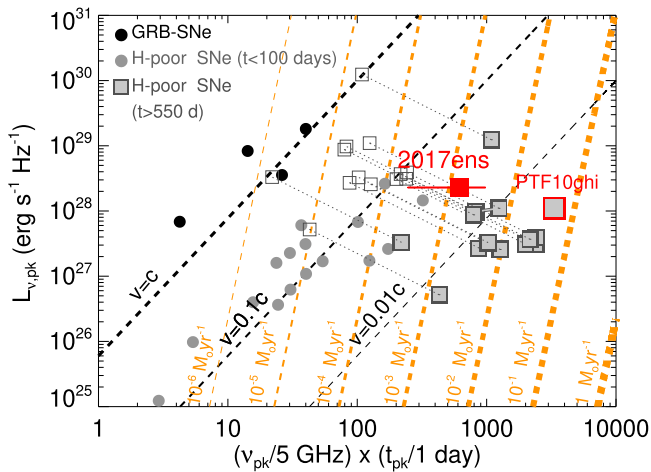


Figure 4. The radio SED at $\delta t = 1334.7\text{--}1374.1$ days constrains the location of SN 2017ens (red square) in the phase space of radio observables, spectral peak luminosity $L_{\nu_{\text{pk}}}$, and $\nu_{\text{pk}} \times t_{\text{pk}}$ (where ν_{pk} is the frequency of the spectral peak at time, t_{pk}). Black (orange) dashed lines mark the location of constant outflow velocity (mass-loss rate \dot{M} , here given for $v_w = 1000 \text{ km s}^{-1}$). GRB-SNe (black circles) show ultrarelativistic outflows and low \dot{M} , while ordinary H-stripped Type Ib/c SNe at $t < 100$ days (gray circles) are associated with slower $v \sim 0.1c$ shocks. The radio properties of SN 2017ens are similar to those of interacting H-stripped SNe at late times $t > 550$ days (gray squares, Stroh et al. 2021), which were detected by the VLASS, Lacy et al. (2020). If ν_{pk} is not constrained, we use an open square to mark the SN location for an assumed optically thin spectrum $F_\nu \propto \nu^{-1}$ and $\nu_{\text{pk}} \approx 0.3 \text{ GHz}$ as in Stroh et al. (2021). The location of the other H-poor SLSN with radio detection at the time of radio discovery (i.e., PTF10ghi, Eftekhari et al. 2019) is marked. This plot assumes equipartition $\epsilon_e = \epsilon_B = 1/3$. References: Soderberg et al. (2012); Stroh et al. (2021).

between electrons and magnetic field, with $\epsilon_e = \epsilon_B = 0.33$, and a geometrical filling factor $f = 0.5$, the observed F_{pk} and ν_{pk} imply a forward-shock radius $R_{\text{FS}} \approx (0.4\text{--}2.0) \times 10^{17} \text{ cm}$ and an average forward shock (FS) shock velocity $v_{\text{FS}}/c \approx (0.01\text{--}0.06)$, which is $v_{\text{FS}} \approx 3700\text{--}18,800 \text{ km s}^{-1}$. The inferred post-shock magnetic field is $B = 0.1\text{--}0.4 \text{ G}$. An equivalent statement for these assumptions is that the CSM density at R_{FS} corresponds to an effective $\dot{M} = (2\text{--}40) \times 10^{-4} M_\odot \text{ yr}^{-1}$ for $v_w = 1000 \text{ km s}^{-1}$, which is a density $\rho_{\text{CSM}} \approx 3 \times 10^{-22}\text{--}1 \times 10^{-19} \text{ g cm}^{-3}$ (particle density in the range $n = 1.7 \times 10^2\text{--}8.0 \times 10^4 \text{ cm}^{-3}$ for pure H composition).²⁸ The inferred shock internal energy is in the range $U_{\text{eq}} \approx (2\text{--}14) \times 10^{48} \text{ erg}$.

Figure 4 shows the location of SN 2017ens at the time of this first radio detection in the $\nu_{\text{pk}}\text{--}L_{\text{pk}}$ plane, comparing it to the locations of other H-stripped core-collapse stellar explosions. Lines of constant shock velocity and mass-loss rates in this figure have been calculated using the equations from DeMarchi et al. (2022).²⁶ SN 2017ens occupies a part of the parameter space that is populated by SNe that showed late-time radio rebrightenings associated with shock interaction with a dense medium. For comparison purposes, we show in Figure 4 the sample of late-time ‘‘SN interactors’’ that were detected by the Very Large Array Sky Survey (VLASS; Lacy et al. 2020), as found by Stroh et al. (2021). In this context, the observed radio properties of SN 2017ens and the implied mass-loss rate are not unprecedented. We note, however, that the low-velocity P-Cygni profiles observed in the optical spectra of SN 2017ens

²⁸ We note that radio observations are sensitive to the CSM density $\rho_{\text{CSM}} \propto \dot{M}/v_w$, which is why we report the assumed v_w for each of the inferred \dot{M} .

indicate a H-rich wind velocity $v_w = 50\text{--}60 \text{ km s}^{-1}$ (Chen et al. 2018), which is significantly slower than the commonly assumed $v_w = 1000 \text{ km s}^{-1}$. The direct implication is that the effective progenitor mass-loss rate at $\sim 10^{17} \text{ cm}$ is $\dot{M} = (0.05\text{--}2) \times 10^{-4} M_\odot \text{ yr}^{-1}$. We note that for these parameters, the optical depth to FFA is $\tau_{\text{ff}} \ll 1$. If the true SSA peak were to be at lower ν and higher F_ν (for example, as a result of FFA) the inferred density would be lower, thus violating the initial FFA assumption. We thus do not include FFA at late times.

Next we discuss the constraints on the innermost region of the CSM at distances $< 10^{17} \text{ cm}$ that can be derived from the radio limits at $\delta t < 1000$ days. In a wind-like CSM density environment $\rho_{\text{CSM}} \propto r^{-2}$ and constant microphysical parameters, the spectral peak frequency and flux density of an SSA spectrum are expected to evolve as $\nu_{\text{pk}} \propto t^{-1}$ and $F_{\text{pk}} \approx \text{constant}$ (Chevalier 1998). Assuming an $F_\nu \propto \nu^{5/2}$ optically thick spectrum and an $F_\nu \propto \nu^{-1}$ optically thin spectrum (as typically observed in SNe, e.g., DeMarchi et al. 2022 and references therein) and extrapolating back in time the radio SED at $\delta t = 1334.7\text{--}1374.1$ days, we find that this model would violate the radio limits at $\delta t \sim 159.7\text{--}305.5$ days. This finding implies a deviation from a pure wind-density profile (e.g., the presence of a shell of dense material encountered by the shock at $\approx R_{\text{FS}}$, which is consistent with the delayed emergence of the H lines in the optical spectra and the flattening of the optical lightcurve) or significant FFA or both. Below we quantify the role of FFA at early times.

We constrain the environment density at $r < 10^{17} \text{ cm}$ using radio observations at $\delta t \leq 306$ days. Self-consistently accounting for the possibility of external FFA in addition to SSA following Weiler et al. (2002), we find that the lack of detectable radio emission at $\delta t \leq 306$ days either implies a large free-free optical depth corresponding to $\dot{M} > 2 \times 10^{-2} M_\odot \text{ yr}^{-1}$ (for an assumed electron temperature $T_e = 10^4 \text{ K}$) or a shock propagation into a lower-density medium with $\dot{M} < 6 \times 10^{-5} M_\odot \text{ yr}^{-1}$ (all mass-loss rates quoted for $v_w = 1000 \text{ km s}^{-1}$). From the flux ratio of the narrow coronal lines [O III] $\lambda 4363$ to $\lambda 5007$ lines at ≈ 215 days, Chen et al. (2018) infer an electron number density in the CSM of $n_e \sim 10^6\text{--}10^8 \text{ cm}^{-3}$ (for an electron temperature $T_e = 50,000\text{--}10,000 \text{ K}$), which translates into an $\dot{M} \sim (0.002\text{--}0.2) M_\odot \text{ yr}^{-1}$ for $v_w = 1000 \text{ km s}^{-1}$ and a shock velocity $\gtrsim 5000 \text{ km s}^{-1}$. We thus favor the high- \dot{M} branch of the radio solution, which is $\dot{M} \approx 10^{-3} M_\odot \text{ yr}^{-1}$ for the more realistic $v_w = 50\text{--}60 \text{ km s}^{-1}$ measured from optical spectra.²⁹ We caution, however, that the optically and radio-emitting regions need not to be the same and that optical emission can originate from significantly higher-density regions, as it has been recently shown for SN 2023ixf (e.g., Berger et al. 2023; Jacobson-Galan et al. 2023). We also note that for these large densities, radio-emitting electrons and positrons may originate from inelastic pp interactions, giving origin to synchrotron emission of secondary pairs from cosmic-ray ions, which is best revealed at millimeter wavelengths (Murase et al. 2014). The late-time emergence of broad H spectral features in SN 2017ens still suggests a shell-like geometry of the H-rich CSM. For a CSM

²⁹ We note that Chen et al. (2018) also report a $\dot{M} \sim 4 \times 10^{-4} M_\odot \text{ yr}^{-1}$ ($v_w = 50 \text{ km s}^{-1}$) from the modeling of the bolometric optical lightcurve at $\delta t > 150$ days. This value is highly dependent on the assumed efficiency of conversion of kinetic energy into radiation, and it is consistent with the electron density that is inferred from the coronal line emission only for $r < 10^{16} \text{ cm}$. Larger \dot{M} would be required to meet the $n_e \sim 10^6\text{--}10^8 \text{ cm}^{-3}$ constraint at $r > 10^{16} \text{ cm}$, which is consistent with our findings.

shell with $\Delta R \approx R_{\text{FS}}$ and the matter density inferred from our radio modeling, we find a total shell mass of $M_{\text{CSM}} \approx 0.5 M_{\odot}$ (order of magnitude estimate).

3.2. Constraints on Relativistic Jets

SN 2017ens displayed broad spectral features with similarities to those observed in gamma-ray burst (GRB) SNe (Chen et al. 2018). GRB-SNe are associated with relativistic jets with a variety of collimation and kinetic energy properties (e.g., Hjorth & Bloom 2012; Corsi & Lazzati 2021) that manifest in the radio phase space as a diverse sample of radio lightcurves spanning ~ 4 orders of magnitude in luminosity (Figure 3, black and gray filled circles). With reference to Figure 3, the limits on the early radio emission of SN 2017ens at $\delta t < 100$ days clearly rule out on-axis jets of cosmological GRBs (gray filled circles) but leave the parameter space of the rapidly decaying radio emission associated with some low-luminosity GRBs unconstrained (e.g., GRBs 060218 and 100316D).

Following Coppejans et al. (2018), we generated a grid of off-axis jet models using high-resolution, two-dimensional relativistic hydrodynamical jet simulations with Boxfit (v2; van Eerten et al. 2012). The synchrotron radio emission originating from the deceleration of the jet in the environment depends on a set of intrinsic and extrinsic physical parameters. We explored isotropic-equivalent jet kinetic energy values in the range $10^{50} \leq E_{\text{k,iso}} \leq 10^{55}$ erg, medium densities $10^{-3} \leq n \leq 10^2 \text{ cm}^{-3}$ for an ISM-like density profile $\rho_{\text{CSM}} \propto r^0$, and mass-loss rates $10^{-8} \leq \dot{M} \leq 10^{-3} M_{\odot} \text{ yr}^{-1}$ ($v_w = 1000 \text{ km s}^{-1}$) for a wind-like profile $\rho_{\text{CSM}} \propto r^{-2}$. We selected jet half-opening angles $\theta_{\text{jet}} = [5^{\circ}, 30^{\circ}]$ as representative of a collimated and less-collimated outflow and observer angles $\theta_{\text{obs}} = [30^{\circ}, 45^{\circ}, 90^{\circ}]$. For fiducial-shock microphysical parameters $\epsilon_e = 0.1$, $\epsilon_B = 0.01$, and $p = 2.5$, our radio observations of SN 2017ens rule out jets with $\theta_{\text{jet}} = 5^{\circ}$ ($\theta_{\text{jet}} = 30^{\circ}$), $E_k \geq 10^{51}$ erg expanding in an ISM-like medium with $n \geq 1 \text{ cm}^{-3}$ ($n \geq 0.1 \text{ cm}^{-3}$) for all observing angles. For a wind-like case, the parts of the parameter space ruled out are $\dot{M} \geq 10^{-4} M_{\odot} \text{ yr}^{-1}$ ($\dot{M} \geq 10^{-5} M_{\odot} \text{ yr}^{-1}$) and $E_k \geq 10^{49.5}$ erg ($E_k \geq 10^{50}$ erg) for $\theta_{\text{jet}} = 5^{\circ}$ ($\theta_{\text{jet}} = 30^{\circ}$) for all θ_{obs} . FFA has a minor impact on these conclusions, as most of the optically thick material is located in regions probed by the jet at times that are before our first epoch of observations.

4. Discussion and Conclusions

We presented the earliest radio detection of an SLSN to date. The combination of the shallower optical lightcurve decay and the late emergence of H emission in the optical spectra of a H-poor SN followed by detectable radio emission strongly suggests an origin of the radio emission related with the interaction of the explosion’s shock with a dense, H-rich medium. Specifically, our radio analysis combined with inferences from high-resolution optical spectroscopy by Chen et al. (2018) suggests the presence of a dense shell of H-rich CSM. We connect the late emergence of the radio emission from SN 2017ens with a combination of the location of the H-rich material and an optical depth effect, i.e., with the time necessary for the radio-emitting shock to reach a radius from which radiation could escape and reach the observer. Assuming spherical geometry, we estimate a CSM mass of $M_{\text{CSM}} \lesssim 0.5 M_{\odot}$ within $\lesssim 10^{17}$ cm.

SN 2017ens belongs to the small group of known H-poor SLSNe that developed H emission in their spectra at $\delta t_{\text{rest}} \geq 100$ days. This sample includes the SLSNe-I, PTF10aagc, PTF10hgi, iPTF13ehe, iPTF15esb, iPTF16bad, and SN 2018bsz (Yan et al. 2015, 2017; Anderson et al. 2018; Chen et al. 2021; Pursiainen et al. 2022). Similar to SN 2017ens, the phenomenology of these transitional SLSNe has been connected with the presence of dense, H-rich CSM at distances of $\sim 10^{16}$ – 10^{17} cm from the explosion site with estimated masses in the range $M_{\text{CSM}} \sim 0.1$ – $3 M_{\odot}$ (see, e.g., Figures 12 and 13 from Brethauer et al. 2022). These properties are not dissimilar to those inferred for transitional SNe that are *not* of superluminous nature (i.e., the “SN2014C-like” events in Brethauer et al. 2022), which suggests that the physical mechanism that drives the pre-SN mass ejections is independent from the superluminous nature of the stellar explosion.

A key open question pertains to the physical origin of the H-rich CSM mass, which is tied to the evolutionary path of the progenitor system in the final years before collapse. The slow CSM velocities ~ 50 – 60 km s^{-1} measured by Chen et al. (2018) from optical spectra are not consistent with the significantly larger escape velocities ($\gtrsim 1000 \text{ km s}^{-1}$) of material from compact H-deficient isolated massive progenitors like Wolf-Rayet stars. Instead, these observations point at the envelope ejection of the primary exploding star as a result of binary interaction following a common-envelope phase (e.g., Podsiadlowski et al. 1992), as was proposed for other transitional objects such as SN 2014C and others (e.g., Milisavljevic et al. 2015; Sun et al. 2020a, 2020b).

The location of the H-rich CSM close to the explosion’s site and the velocities measured imply an envelope ejection within ≈ 500 yr of core collapse. While the statistics are not complete, based on current optical spectroscopy observations, the fraction of SLSNe-I displaying a late-time emergence of H-features is of the order of $\lesssim 1/10$ (P. Blanchard 2023, private communication). This fraction is broadly consistent with the expectations from a population of binary progenitor systems with a diverse set of initial properties and where only a small fraction of systems with wide orbital separations experience common-envelope evolution and envelope ejection in the centuries before the collapse of the primary star. For example, Podsiadlowski et al. (1992) estimate that $\sim 6\%$ of binary systems with a primary star massive enough to explode as an SN experience “case-C” mass transfer (i.e., the progenitor fills its Roche lobe in a late evolutionary stage, which is associated with late-time envelope ejection). Updated binary synthesis simulations point at a fraction in the range 4%–10% of progenitors of H-stripped SNe resulting from systems that experienced case-C common-envelope evolution, with the range of values reflecting the assumed slope of the initial-mass function (Margutti et al. 2017). This suggests that (i) interacting binary systems might be common progenitors of SLSNe-I and (ii) the physical ingredient that determines the superluminous nature of an SN (which constitutes $\approx 0.2\%$ of the core-collapse SN rate by volume in the local Universe; Li et al. 2011; Quimby et al. 2013) is likely independent of the mechanism that leads to hydrogen envelope removal, which can instead operate in a wide variety of primary stars/progenitor systems.

Finally, we address the implications of our deep constraints on the presence of relativistic jets in SN 2017ens in the broader context of radio observations of SLSNe-I. SN 2017ens and PTF10hgi are the only two SLSNe-I for which radio emission

has been detected (Figure 3). The late-time 6 GHz radio detection of PTF10hgi at $\delta t_{\text{rest}} \approx 6.3$ yr has been interpreted as emission from an off-axis jet (Eftekhari et al. 2019), but the favored interpretation, based on the radio spectrum, is that of the emergence of emission from a pulsar wind nebula inflated by a magnetar central engine (Eftekhari et al. 2019; Law et al. 2019; Mondal et al. 2020). At the time of writing, SN 2011kl associated with GRB 111209A is the only known example of stellar explosion that satisfies the superluminous criterion and that has harbored a relativistic jet (Greiner et al. 2015). Constraints on relativistic jets in a population of optically discovered SLSNe-I have been presented in Coppejans et al. (2018) and Eftekhari et al. (2021). The deep multiyear radio campaign on SN 2017ens provides additional insight. While low-energy outflows with $E_k \leq 10^{50}$ erg similar to those associated with low-luminosity GRBs (e.g., Berger et al. 2003; Soderberg et al. 2006; Cano 2013; Margutti et al. 2013) are not constrained, radio observations of SN 2017ens rule out energetic jets with properties similar to cosmological long GRBs expanding in environments typical of massive stars ($\dot{M} \geq 10^{-5} M_{\odot} \text{ yr}^{-1}$) for all observing angles, suggesting that either the CSM density along the jet direction is lower than around a typical massive star (and lower than our inferences of Section 3) or that SN 2017ens did not launch such a jet.

The phase-space available to hide off-axis relativistic jets in SLSNe-I has significantly shrunk as a result of dedicated multiyear radio campaigns on the nearest SLSNe. Going forward, the very early identification of SLSNe, within days of explosion, will allow us to probe the weakest mildly relativistic jets (like those of GRBs 060218 and 100316D, Figure 3). Our SN 2017ens effort highlights the scientific return of consistent and persistent radio monitoring of SLSNe from days until several years after the explosion, *even in the case of radio non-detections in the first years*. Coupled with deep high-resolution

optical spectroscopy that can reveal the chemical composition and dynamics of the CSM (Chen et al. 2018), the radio emission from SN shocks provides a unique window into the final moments of evolution of massive stars that would not be otherwise accessible.

Acknowledgments

We thank the anonymous referee for suggestions, which helped make the manuscript clearer. The National Radio Astronomy Observatory is a facility of the National Science Foundation operated under cooperative agreement by Associated Universities, Inc. The TReX team at UC Berkeley is supported in part by the National Science Foundation under grant No. AST-2221789 and AST-2224255, and by the Heising-Simons Foundation under grant # 2021-3248. T.E. is supported by NASA through the NASA Hubble Fellowship grant HST-HF2-51504.001-A awarded by the Space Telescope Science Institute, which is operated by the Association of Universities for Research in Astronomy, Inc., for NASA, under contract NAS5-26555. M.R.D. acknowledges support from the NSERC through grant RGPIN-2019-06186, the Canada Research Chairs Program, the Canadian Institute for Advanced Research (CIFAR), and the Dunlap Institute at the University of Toronto. M.N. is supported by the European Research Council (ERC) under the European Union’s Horizon 2020 research and innovation program (grant agreement No. 948381) and by UK Space Agency grant No. ST/Y000692/1.

Appendix Radio Data Table

Table 1 shows radio observations of SN2017ens.

Table 1
VLA Observations of SN 2017ens





Start Date (dd/mm/yy)	Project ID	VLA Config.	Centroid MJD	Phase ^a (days)	Frequency (GHz)	Bandwidth (GHz)	Flux Density ^b (μJy)	Rms ($\mu\text{Jy beam}^{-1}$)
28/07/2017	17A-480	C	57,962.839	55.039	6	2	<22	7.3
19/08/2017	17A-480	C	57,984.785	76.985	22	8	<23	7.6
19/08/2017	17A-480	C	57,984.818	77.018	6	2	<17	5.7
10/11/2017	17B-225	B	58,067.521	159.721	22	8	<29	9.7
05/04/2018	17B-225	A	58,213.270	305.470	22	8	<26	8.7
28/01/2021	20B-144	A	59,242.481	1334.681	22	8	<18	5.9
28/01/2021	20B-144	A	59,242.515	1334.715	6	4	38 ± 5	4.7
05/02/2021	20B-144	A	59,250.306	1342.506	10	4	25 ± 6	6.5
05/02/2021	20B-144	A	59,250.329	1342.529	3	2	46 ± 7	7.3
05/02/2021	20B-144	A	59,250.352	1342.552	1.5	1	<45	15
22/10/2021	21B-290	B	59,509.742	1601.942	10	4	38 ± 6	6.4
22/10/2021	21B-290	B	59,509.759	1601.959	6	4	22 ± 8	7.8
22/10/2021	21B-290	B	59,509.775	1601.975	3	2	<35	11.6
22/10/2021	21B-290	B	59,509.791	1601.991	1.5	1	<96	32.0

Notes.

^a Days since explosion (which is MJD 57,907.8), using the midpoint time of the exposure on source.

^b Uncertainties are 1σ , and upper limits are 3σ . The listed uncertainties take a systematic uncertainty of 5% into account. We fit a point source to the image (i.e., an elliptical Gaussian with the same dimensions as the restoring beam) to derive the flux density after our detection at C-band on 2021 January 28 and give the fitted flux density. If this is not formally a 3σ detection, we give the 3σ upper limit.

ORCID iDs

Raffaella Margutti  <https://orcid.org/0000-0003-4768-7586>
 J. S. Bright  <https://orcid.org/0000-0002-7735-5796>
 D. J. Matthews  <https://orcid.org/0000-0002-4513-3849>
 D. L. Coppejans  <https://orcid.org/0000-0001-5126-6237>
 K. D. Alexander  <https://orcid.org/0000-0002-8297-2473>
 E. Berger  <https://orcid.org/0000-0002-9392-9681>
 M. Bietenholz  <https://orcid.org/0000-0002-0592-4152>
 R. Chornock  <https://orcid.org/0000-0002-7706-5668>
 L. DeMarchi  <https://orcid.org/0000-0003-4587-2366>
 M. R. Drout  <https://orcid.org/0000-0001-7081-0082>
 T. Eftekhari  <https://orcid.org/0000-0003-0307-9984>
 W. V. Jacobson-Galan  <https://orcid.org/0000-0002-3934-2644>
 T. Laskar  <https://orcid.org/0000-0003-1792-2338>
 D. Milisavljevic  <https://orcid.org/0000-0002-0763-3885>
 K. Murase  <https://orcid.org/0000-0002-5358-5642>
 M. Nicholl  <https://orcid.org/0000-0002-2555-3192>
 C. M. B. Omand  <https://orcid.org/0000-0002-9646-8710>
 M. Stroh  <https://orcid.org/0000-0002-3019-4577>
 G. Terreran  <https://orcid.org/0000-0003-0794-5982>

References

- Anderson, J. P., Pessi, P. J., Dessart, L., et al. 2018, *A&A*, 620, A67
 Berger, E., Keating, G. K., Margutti, R., et al. 2023, *ApJL*, 951, L31
 Berger, E., Kulkarni, S. R., Pooley, G., et al. 2003, *Natur*, 426, 154
 Bose, S., Dong, S., Pastorello, A., et al. 2018, *ApJ*, 853, 57
 Brethauer, D., Margutti, R., Milisavljevic, D., et al. 2022, *ApJ*, 939, 105
 Bright, J., Mooley, K., Fender, R., et al. 2017, *ATel*, 10538, 1
 Cano, Z. 2013, *MNRAS*, 434, 1098
 CASA Team, Bean, B., Bhatnagar, S., et al. 2022, *PASP*, 134, 114501
 Chandra, P., Bera, A., Biswas, A., et al. 2021, *ATel*, 14448, 1
 Chandra, P., & Frail, D. A. 2012, *ApJ*, 746, 156
 Chandra, P., Ofek, E. O., Frail, D. A., et al. 2009, *ATel*, 2241, 1
 Chandra, P., Ofek, E. O., Frail, D. A., et al. 2010, *ATel*, 2367, 1
 Chen, T. W., Brennan, S. J., Wesson, R., et al. 2021, arXiv:2109.07942
 Chen, T. W., Inserra, C., Fraser, M., et al. 2018, *ApJL*, 867, L31
 Chevalier, R. A. 1998, *ApJ*, 499, 810
 Chevalier, R. A., & Fransson, C. 2017, in *Handbook of Supernovae*, ed. A. W. Alsabti & P. Murdin (Berlin: Springer), 875
 Chevalier, R. A., & Irwin, C. M. 2011, *ApJL*, 729, L6
 Chomiuk, L., Chornock, R., Soderberg, A. M., et al. 2011, *ApJ*, 743, 114
 Coppejans, D. L., Margutti, R., Guidorzi, C., et al. 2018, *ApJ*, 856, 56
 Coppejans, D. L., Matthews, D., Margutti, R., et al. 2021a, *TNSAN*, 66, 1
 Coppejans, D. L., Matthews, D., Margutti, R., et al. 2021b, *ATel*, 14418, 1
 Corsi, A., & Lazzati, D. 2021, *NewAR*, 92, 101614
 DeMarchi, L., Margutti, R., Dittman, J., et al. 2022, *ApJ*, 938, 84
 Eftekhari, T., Berger, E., Margalit, B., et al. 2019, *ApJL*, 876, L10
 Eftekhari, T., Margalit, B., Omand, C. M. B., et al. 2021, *ApJ*, 912, 21
 Fransson, C., Ergon, M., Challis, P. J., et al. 2014, *ApJ*, 797, 118
 Gal-Yam, A. 2019, *ARA&A*, 57, 305
 Gal-Yam, A., Mazzali, P., Ofek, E. O., et al. 2009, *Natur*, 462, 624
 Greiner, J., Mazzali, P. A., Kann, D. A., et al. 2015, *Natur*, 523, 189
 Hatsukade, B., Tominaga, N., Hayashi, M., et al. 2018, *ApJ*, 857, 72
 Hatsukade, B., Tominaga, N., Morokuma, T., et al. 2021a, *ApJ*, 922, 17
 Hatsukade, B., Tominaga, N., Morokuma, T., et al. 2021b, *ApJL*, 911, L1
 Hjorth, J., & Bloom, J. S. 2012, in *Gamma-Ray Bursts*, ed. C. Kouveliotou, A. M. J. Wijers, & S. Woosley, Vol. 51 (Cambridge: Cambridge Univ. Press), 169
 Jacobson-Galan, W. V., Dessart, L., Margutti, R., et al. 2023, arXiv:2306.04721
 Kasen, D., & Bildsten, L. 2010, *ApJ*, 717, 245
 Kasliwal, M. M., Cenko, S. B., Singer, L. P., et al. 2016, *ApJL*, 824, L24
 Lacy, M., Baum, S. A., Chandler, C. J., et al. 2020, *PASP*, 132, 035001
 Law, C. J., Omand, C. M. B., Kashiyama, K., et al. 2019, *ApJ*, 886, 24
 Li, W., Bloom, J. S., Podsiadlowski, P., et al. 2011, *Natur*, 480, 348
 Margutti, R., Kamble, A., Milisavljevic, D., et al. 2017, *ApJ*, 835, 140
 Margutti, R., Milisavljevic, D., Soderberg, A. M., et al. 2014, *ApJ*, 797, 107
 Margutti, R., Soderberg, A. M., Wieringa, M. H., et al. 2013, *ApJ*, 778, 18
 McMullin, J. P., Waters, B., Schiebel, D., Young, W., & Golap, K. 2007, in *ASP Conf. Ser. 376, Astronomical Data Analysis Software and Systems XVI*, ed. R. A. Shaw, F. Hill, & D. J. Bell (San Francisco, CA: ASP), 127
 Milisavljevic, D., Margutti, R., Kamble, A., et al. 2015, *ApJ*, 815, 120
 Mondal, S., Bera, A., Chandra, P., & Das, B. 2020, *MNRAS*, 498, 3863
 Moriya, T. J., Sorokina, E. I., & Chevalier, R. A. 2018, *SSRv*, 214, 59
 Murase, K., Thompson, T. A., & Ofek, E. O. 2014, *MNRAS*, 440, 2528
 Nicholl, M., Berger, E., Smartt, S. J., et al. 2016, *ApJ*, 826, 39
 Nicholl, M., Blanchard, P. K., Berger, E., et al. 2018, *ApJL*, 866, L24
 Offringa, A. R., & Smirnov, O. 2017, *MNRAS*, 471, 301
 Omand, C. M. B., & Jerkstrand, A. 2023, *A&A*, 673, A107
 Podsiadlowski, P., Joss, P. C., & Hsu, J. J. L. 1992, *ApJ*, 391, 246
 Pursiainen, M., Leloudas, G., Paraskeva, E., et al. 2022, *A&A*, 666, A30
 Quimby, R. M., Kulkarni, S. R., Kasliwal, M. M., et al. 2011, *Natur*, 474, 487
 Quimby, R. M., Yuan, F., Akerlof, C., & Wheeler, J. C. 2013, *MNRAS*, 431, 912
 Schulze, S., Krühler, T., Leloudas, G., et al. 2018, *MNRAS*, 473, 1258
 Soderberg, A. M., Chakraborti, S., Pignata, G., et al. 2010, *Natur*, 463, 513
 Soderberg, A. M., Kulkarni, S. R., Nakar, E., et al. 2006, *Natur*, 442, 1014
 Soderberg, A. M., Margutti, R., Zauderer, B. A., et al. 2012, *ApJ*, 752, 78
 Stroh, M. C., Terreran, G., Coppejans, D. L., et al. 2021, *ApJL*, 923, L24
 Sun, L., Xiao, L., & Li, G. 2022, *MNRAS*, 513, 4057
 Sun, N.-C., Maund, J. R., & Crowther, P. A. 2020a, *MNRAS*, 497, 5118
 Sun, N.-C., Maund, J. R., Hirai, R., Crowther, P. A., & Podsiadlowski, P. 2020b, *MNRAS*, 491, 6000
 Tinyant, S., Lau, R. M., Kasliwal, M. M., et al. 2019, *ApJ*, 887, 75
 Tonry, J. L., Denneau, L., Heinze, A. N., et al. 2018, *PASP*, 130, 064505
 van Eerten, H., van der Horst, A., & MacFadyen, A. 2012, *ApJ*, 749, 44
 Weiler, K. W., Panagia, N., Montes, M. J., & Sramek, R. A. 2002, *ARA&A*, 40, 387
 Woosley, S. E. 2010, *ApJL*, 719, L204
 Yan, L., Lunnan, R., Perley, D. A., et al. 2017, *ApJ*, 848, 6
 Yan, L., Quimby, R., Ofek, E., et al. 2015, *ApJ*, 814, 108